

Piezoelectric Transducer Design for Simultaneous Ultrasonic Power Transfer and Backscatter Communication

Ahmed Allam*, Karim Sabra, and Alper Erturk

G.W. Woodruff School of Mechanical Engineering, Georgia Institute of Technology,
Atlanta, GA, USA

E-mail: *a.allam@gatech.edu

Abstract. Ultrasonic waves can transfer power and data to sensors and devices deployed to traditionally inaccessible locations, such as inside the human body or deep in the ocean, eliminating the need for battery replacement. In ultrasonic power and data transfer systems, a piezoelectric transducer converts incident ultrasonic waves to useful electric power while transmitting data by modulating its reflected signal through backscatter communication. Existing approaches rely on reflecting a portion of the incident power to communicate, reducing the harvested power. This work realizes uninterrupted power harvesting with simultaneous backscatter communication through frequency multiplexing. A piezoelectric transducer is first designed and tested experimentally for high sensitivity and high bandwidth operation through low-loss broadband acoustic and electrical impedance matching. The transducer achieved 70% bandwidth at 1 MHz with a 10 dB difference between reflecting and absorbing incident ultrasonic waves. A frequency multiplexing technique is then developed to separate power and data into different frequency bands achieving simultaneous operation. The technique extends the range and bandwidth of ultrasonically powered devices such as biomedical implants and ocean monitoring sensors.

Submitted to: *Smart Mater. Struct.*

1. Introduction

Ultra-low-power electronic circuits and sensors enable devices to be deployed in traditionally inaccessible locations such as inside the brain [1], in sealed metallic enclosures [2], or deep in the ocean [3, 4]. The inaccessibility of these environments limits battery operation which motivated researchers to consider ultrasonic waves for transmitting both power and data to the device. Ultrasonic waves solve various challenges in different research domains from medicine to defense industry, and the solutions developed for each field exhibit similarities.

Biomedical technology researchers use ultrasonic waves for powering and communicating with implanted medical devices (IMDs)[5] for health monitoring [6,

7, 8, 9, 10, 11], enhancing tumor treatment [12, 13], neural recording [1, 14], and neural stimulation [15, 16, 17, 18, 19, 20, 21]. Ultrasonic power is utilized since the United States food and drugs administration (FDA) limits the electromagnetic power transmitted through the human body to 0.1 mW mm^{-2} . In contrast, ultrasonic waves can have a power density as high as 7.2 mW mm^{-2} [22]. Ultrasonic waves also have a smaller wavelength than electromagnetic waves, allowing for smaller implants. Ultrasonic power delivery and communication is one of the enabling technologies for concepts such as the body area network (BAN) [23, 24].

Ultrasonic waves are also investigated for deep underwater communication solutions [25]. While optical and RF-based solutions exist, their operation is typically limited to short links due to the large attenuation of electromagnetic waves underwater [26, 25]. Underwater wireless ultrasonic sensor nodes are investigated for ocean monitoring and tracking climate change [27, 28], increasing underwater communication bandwidth [29], tracking marine life [30, 31, 32], and as markers for aiding the navigation of autonomous underwater vehicles [33]. Most of the devices developed in the underwater literature are battery-operated, limiting their lifespan given the difficulties in retrieving and replacing the batteries. However, recent efforts have investigated ultrasonic waves for both powering and communicating with underwater sensor nodes [3, 4, 34, 35].

Researchers have also investigated ultrasonic power and data transfer (UPDT) through metals [36, 37, 38, 39, 40, 2, 41, 42]. Since RF waves cannot penetrate thick metallic enclosures, mechanical waves remain the only power and data transfer approach. Sealed metallic enclosures equipped with UPDT systems protects sensitive electronics from electromagnetic interference, and provides complete weather protection.

All UPDT systems reviewed in the literature included a PZT transmitter (TX) connected to an electrical power source. The power and data are transmitted to a piezoelectric receiver (RX) connected to either a sensor (for collecting data) or an actuator (for stimulating its environment). The data can flow from the transmitter to the receiver (downlink communication for sending excitation commands) [15, 2, 16, 18, 20, 43], from the receiver to the transmitter (uplink communication to transmit sensor data and device status) [6, 44, 45, 1, 14, 8, 41, 42, 4, 46, 10, 11], or in both directions either simultaneously (full-duplex) [47, 40] or in turns (half-duplex/time multiplexing) [48, 49, 50, 36, 51, 21]. Downlink communication can be as simple as switching between turning the transmitter on and off, i.e., on-off keying (OOK) [16] or using advanced modulation schemes such as orthogonal frequency division multiplexing (OFDM) for higher throughput [2].

Uplink communication has more restrictions than downlink since the power available to the wireless device is limited. While active approaches (exciting the transducer to send data) have been proposed for uplink communication, their realization usually involves toggling between storing enough power and transmitting the uplink data [8, 4]. Since no communication occurs while the wireless device is being charged, the uplink throughput is limited. It also requires a large capacitor or a battery to store

the data, which might not be feasible in space-limited applications such as biomedical implants.

Ultrasonic backscatter is a passive uplink communication approach in which the reflected ultrasonic signal from RX is modulated to send the uplink data. In backscatter communication, the electrical impedance connected to the piezoelectric receiver is modulated, changing the receiver's acoustic impedance and the amplitude of the reflected ultrasonic signal. By switching between absorbing and reflecting the ultrasonic waves, as shown in Fig.1a, uplink communication is established with minimal power from RX. Only a low-power transistor (with its driving circuit) provides uplink communication using backscatter reducing hardware complexity compared to active approaches. The majority of the surveyed literature incorporated backscattering in their UPDT designs [48, 40, 34, 10].

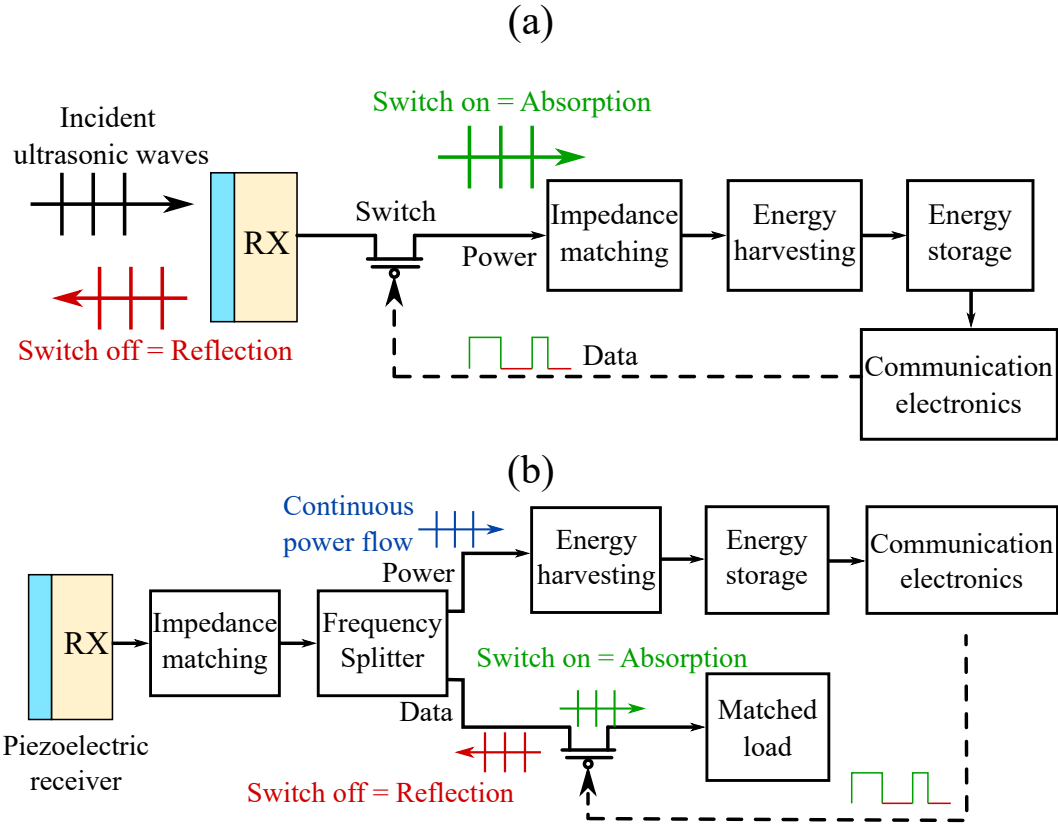


Figure 1. (a) Existing implementation of ultrasonic power and data transfer in literature. (b) Proposed system for simultaneous power and data transfer based on frequency multiplexing.

State-of-the-art UPDT systems reflect a portion of the incident ultrasonic power to establish backscatter communication limiting the amount of ultrasonic power they can absorb. As shown in Fig.1a, when the transistor is on, ultrasonic power flows to the energy harvesting circuit (rectification and voltage regulation) and is stored for the device operation. However, no power is harvested when the transistor is off,

and most of the incident acoustic power is reflected. Ozeri et al. [45] attempted to address this issue by introducing a slight change in the load connected to the transducer instead of completely shorting it. Still, their approach only compromised communication sensitivity and power harvesting.

This work realizes uninterrupted power harvesting with simultaneous backscatter communication through frequency multiplexing. A frequency band is dedicated to continuous power transfer and isolated from the data frequency bands. As shown in Fig.1b, the signal is split using a frequency splitter (also known as a diplexer in RF literature or frequency crossover in audio literature), and power is supplied continuously to an energy harvesting circuit uninterrupted by switching the data channel. However, in order to achieve frequency multiplexing, the piezoelectric receiver must have both high bandwidth and sensitivity which can be achieved through careful broadband impedance matching of the piezoelectric transducer to both the acoustic and electric domains.

We first introduce a simplified analytical model for analyzing the reflection from a piezoelectric layer in Sec. 2. Simultaneous acoustic and electric impedance matching of an air-backed piezoelectric transducer is then discussed in Sec. 3. Several air-backed transducers are then fabricated, and their performance is characterized in Sec. 4 to evaluate the quality of the acoustic matching layers. Finally, the transducer is electrically matched for broadband data transfer and uninterrupted power delivery in Sec. 5.

2. Modeling Reflection from a Piezoelectric Layer

Consider a transducer made of a thin piezoelectric disc transducer of thickness h_p and area A_p . The transducer is poled in the thickness direction with thin electrodes plated on each face. Fig. 2 shows the transducer connected to an electric load with equivalent complex electrical impedance Z_e . The front face of the transducer is submerged underwater, and its back is in contact with a material with mechanical impedance Z_b . The impedance matrix (\mathbf{Z}) of the transducer relates the input forces on the front and back faces (F_1, F_2) and voltage (V_3) to the velocities (v_1, v_2) and current (I_3). \mathbf{Z} is given by [52]:

$$\begin{bmatrix} F_1 \\ F_2 \\ V_3 \end{bmatrix} = -j \underbrace{\begin{bmatrix} Z_p \cot(k_p h_p) & Z_p \csc(k_p h_p) & \frac{\bar{h}_{33}}{\omega} \\ Z_p \csc(k_p h_p) & Z_p \cot(k_p h_p) & \frac{\bar{h}_{33}}{\omega} \\ \frac{\bar{h}_{33}}{\omega} & \frac{\bar{h}_{33}}{\omega} & \frac{1}{\omega C_p} \end{bmatrix}}_{\mathbf{Z}} \begin{bmatrix} v_1 \\ v_2 \\ I_3 \end{bmatrix}, \quad (1)$$

where $Z_p = \rho_p c_p A_p$ is the mechanical impedance of the piezoelectric layer, ρ_p is the density, c_p is the longitudinal wave speed, $\bar{h}_{33} = e_{33}/\epsilon_{33}^s$ is known as the transmitting coefficient, e_{33} is the piezoelectric voltage constant, ϵ_{33}^s is the permittivity at constant strain, $k_p = \omega/c_p$ is the wavenumber in the piezoelectric layer, and $C_p = \epsilon_{33}^s A_p/h_p$ is the piezoelectric layer capacitance at constant strain (i.e., when mechanically clamped).

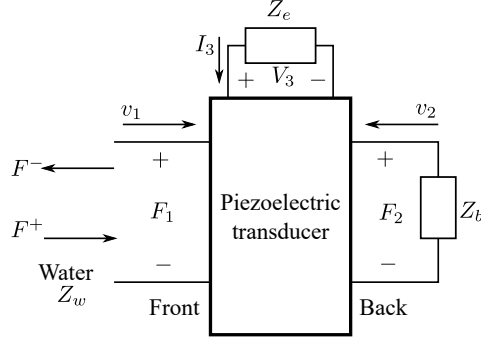


Figure 2. A schematic of a piezoelectric disc transducer represented as a 3-port element connected to arbitrary electrical impedance Z_e and an arbitrary backing layer with mechanical impedance Z_b .

The electrical and backing impedance yield the equations:

$$F_2 = -v_2 Z_b \quad (2)$$

$$V_3 = -I_3 Z_e \quad (3)$$

which are substituted in Eq. 1 to find the input mechanical impedance of the transducer Z_{in} :

$$\begin{aligned} Z_{in} &= \frac{F_1}{v_1} \\ &= Z_{11} - \frac{Z_{12}^2 - \frac{Z_{12}Z_{13}^2}{Z_e + Z_{33}}}{Z_b + Z_{11} - \frac{Z_{13}^2}{Z_e + Z_{33}}} - \frac{Z_{13}^2 - \frac{Z_{12}Z_{13}^2}{Z_b + Z_{11}}}{Z_e + Z_{33} - \frac{Z_{13}^2}{Z_b + Z_{11}}} \end{aligned} \quad (4)$$

where Z_{mn} are the elements of the impedance matrix. The value of Z_{in} determines the amount of acoustic reflection from the transducer. Equation 4 shows that Z_{in} is a function of the transducer geometry and material, the backing layer impedance, and the electrical impedance. By changing the electrical impedance connected to the transducer, its mechanical impedance changes enabling backscatter communication.

The amount of reflection is calculated using the complex reflection coefficient of the piezoelectric transducer (S_{11}) by assuming incident and reflected mechanical waves F^+, F^- on the front face of the transducer, as shown in Fig. 2. The incident and reflected waves are related to the total force and velocity by:

$$\begin{aligned} F_1 &= F^+ + F^- \\ v_1 &= \frac{F^+ - F^-}{Z_w} \end{aligned} \quad (5)$$

where $Z_w = \bar{Z}_w A_p$ and \bar{Z}_w is the characteristic acoustic impedance of water in Rayleighs. The complex reflection coefficient (S_{11}) is defined as:

$$S_{11} = \frac{F^-}{F^+} \quad (6)$$

By solving Eq. 4 and Eq. 5 together, the complex reflection coefficient of the transducer with respect to water is given by:

$$S_{11} = \frac{Z_w - Z_{in}}{Z_w + Z_{in}} \quad (7)$$

This equation assumes that the piezoelectric layer is in direct contact with water. If acoustic matching layers are present, the transfer matrix method is used to calculate the reflection from the matched transducer [53].

The Smith chart is a useful tool for visualizing the complex reflection coefficient (S_{nn}). Since the magnitude of the reflection coefficient cannot be greater than one, all its possible values are inside the unit circle, and thus the shape of the chart is circular as shown in Fig. 3. A reflection coefficient value close to the origin of the chart represents low reflection, and therefore a better match to a reference impedance. For acoustic ports, the reference impedance is the mechanical impedance of the medium in which the transducer will operate, such as water, tissue, or metal. For electric ports, this reference impedance is commonly chosen to be 50Ω in RF circuits; however, it can be set to the impedance of any electric load that needs to be powered.

Impedance matching aims to minimize the reflection coefficient by adding electrical or mechanical elements that shifts the system's impedance towards the center of the plot. The horizontal line in the middle of the chart represents a purely resistive impedance, while the top and bottom halves represent inductive and capacitive impedance, respectively. Lines of constant resistance, reactance, conductance, and susceptance can be shown on the chart to guide the impedance matching efforts. All the values displayed on the chart are normalized to the chosen reference impedance. A more comprehensive discussion of the Smith chart can be found elsewhere in the existing literature. Ref. [54].

3. Acoustic and Electrical Impedance Matching of Piezoelectric Transducers

A 1 MHz piezoelectric disc transducer of thickness 2.1 mm and diameter 30 mm is selected to demonstrate simultaneous acoustic and electrical impedance matching. The transducer is made of a hard piezoelectric material (PZT-4) since it has a high piezoelectric coefficient and low damping to maximize coupling and minimize the power dissipated. The material properties of the piezoelectric layer are summarized in Table 1.

The backing layer of common commercial transducers is usually made of a lossy material with impedance close to PZT which is well suited for imaging applications. This backing approach increases the transducer's bandwidth at the expense of lower sensitivity. Nearly half the input power to the transducer is lost to the backing layer in this configuration. To avoid power loss to the transducer backing, air backing is used since it has a large impedance mismatch with PZT-4, which increases the efficiency

Table 1. Material properties of PZT-4 used in the transducer 1D model.

Property	ρ_p	c_p	\bar{h}_{33}	C_{33}^D	C_p	Q_m	$\tan \delta$
Unit	kg/m ³	m/s	kV/mm	GPa	nF	-	%
Value	7500	4706	2727	166	1.98	500	0.4

and sensitivity of the transducer. Next, the transducer bandwidth is enhanced through simultaneous electrical and acoustic impedance matching.

Fig. 3 shows the steps for enhancing the bandwidth and sensitivity of an air-backed transducer using electrical and acoustic impedance matching. The transducer is modeled using the transfer matrix method, and its impedance and reflection characteristics were simulated using MATLAB. First, the air-backed transducer without impedance matching is shown on the Smith chart (Fig. 3a&b) as solid blue lines. The electrical impedance of the bare transducer appears as a large circle which complicates electrical matching efforts since the impedance varies between a wide range of capacitive and inductive values depending on the frequency. The electrical impedance variation is reduced when the acoustic port is matched to water by shifting the acoustic impedance in Fig. 3a closer to the origin using quarter wavelength matching layers as commonly done in the literature [55].

In the literature, a single quarter wavelength matching layer is commonly used to match piezoelectric transducers to water. The material for a quarter wavelength matching layer needs to have an acoustic impedance at the geometric mean of the two mediums that need to be matched, i.e., for matching a piezoelectric transducer to water:

$$Z_m = \sqrt{Z_p Z_w} \quad (8)$$

where $Z_m = 7$ MRayl is the acoustic impedance of the single matching layer. However, low-loss natural materials with an acoustic impedance close to 7 MRayl are rare, limiting the usefulness of single matching layers in high sensitivity/low loss applications such as UPDT [56]. Alternatively, two quarter wavelength layers can be used to enhance the piezoelectric transducer's bandwidth [57, 56]. The impedance of each matching layer is calculated from [58]:

$$Z_{m1} = Z_p^{2/3} Z_w^{1/3} \quad (9)$$

$$Z_{m2} = Z_p^{1/3} Z_w^{2/3} \quad (10)$$

where Z_{m1} is the matching layer adjacent to the transducer, and Z_{m2} is adjacent to water. The acoustic impedance of quartz glass is around 12.1 MRayl which is very close to Z_{m1} value from Eq. 9. The value calculated for Z_{m2} is 4.3 MRayl, which lies in the neighborhood of metal-filled epoxies such as silver epoxy or tungsten-filled epoxy. These materials, however, are lossy and may reduce the sensitivity of the transducer. Pure epoxy (3 MRayl) has lower attenuation and is easy to cast and polish to exact thickness

for fine-tuning the matching process, so it was used instead. Epotek-301 is a clear epoxy commonly used in the ultrasound literature because of its low viscosity, which allows it to be easily cast without trapping air bubbles.

The acoustic and electrical reflection coefficients for a two-layer matched transducer are shown as dot-dashed yellow lines in Fig. 3. The electrical impedance variation was reduced significantly after the acoustic impedance matching, as shown in Fig. 3b. The electrical impedance is shifted to the center of the Smith chart to match the transducer electrically. A 6 μH series inductor and a 15 μH parallel inductor were used, as indicated in Fig. 3b. Fig. 3c shows that the matched transducer achieves a wide flat bandwidth close to 80% with a large sensitivity.

Fig. 3d shows the acoustic reflection from the transducer in the time domain. A Gaussian pulse centered around 1 MHz with a bandwidth of 50% is incident on the transducer, and the reflected pulses are analyzed. The impedance-matched transducer converts most of the incident pulse into electrical energy, and a much smaller pulse is reflected compared to the bare transducer.

4. Experimental Verification

A set of transducers (M1-M3) were fabricated with two acoustic matching layers, as discussed in Sec. 3. The epoxy layer was varied between 0.65-0.75 mm to obtain a transducer with the best possible match between the electrical and the acoustic domains. Additionally, an air-backed transducer without acoustic matching (U1) was fabricated to act as a baseline. The dimensions of the fabricated transducers are summarized in Table 2.

Table 2. Dimensions of the fabricated transducers.

Layer	Unit	U1	M1	M2	M3
PZT	mm	2.1	2.1	2.1	2.1
Epoxy	μm	-	10	10	10
Quartz glass	mm	-	1.6	1.6	1.56
Epotek 301	mm	-	0.4	0.5	0.6

4.1. Transducer fabrication

The transducers casings were 3D printed using an Ultimaker 3 printer. The casings shown in Fig. 4 were designed to provide air backing to the transducers by only

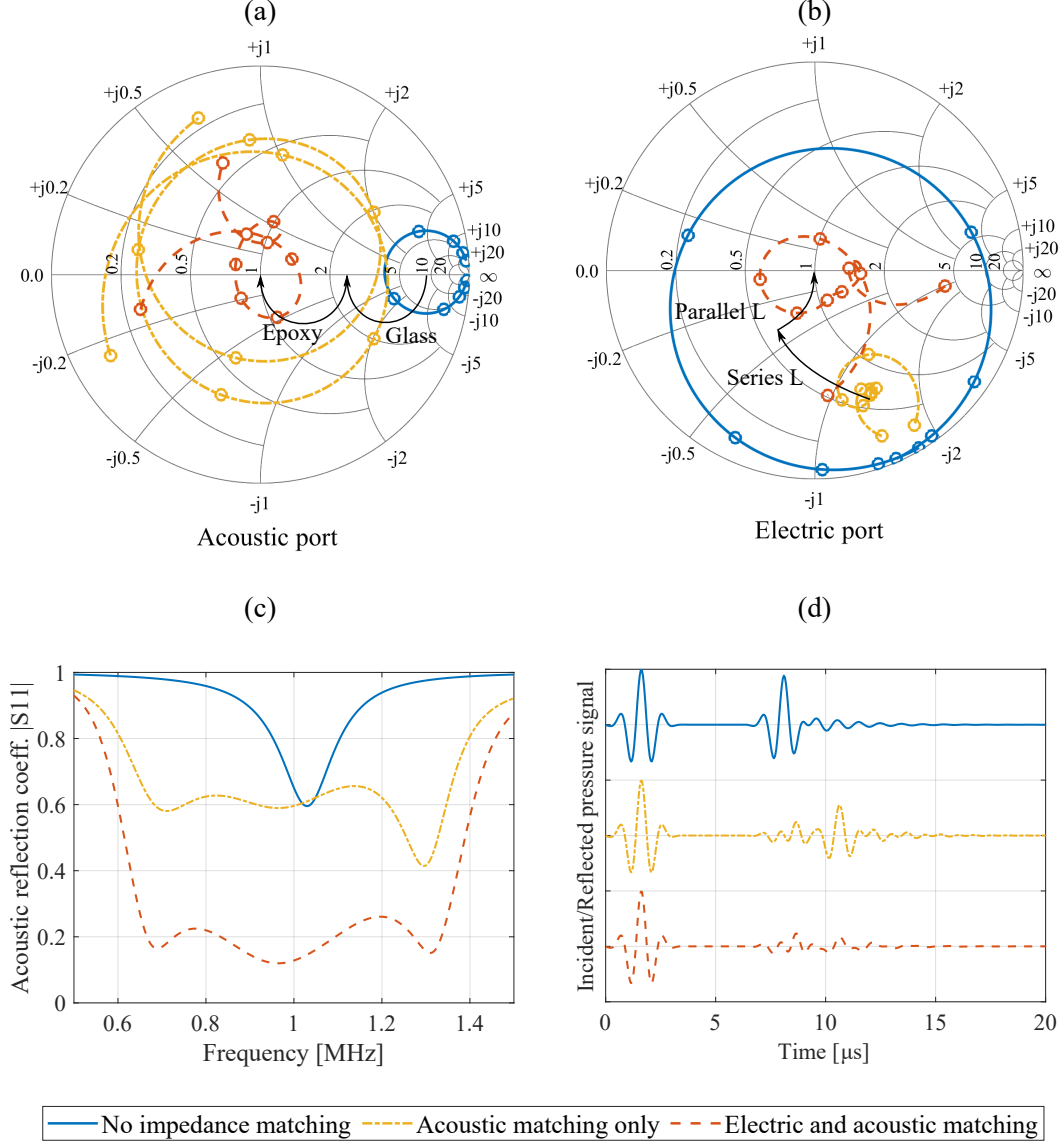


Figure 3. Smith charts of the analytical (a) acoustic and (b) electric reflection coefficients of the developed piezoelectric transducer showing the impedance matching steps. The amplitude of the acoustic reflection is shown for each step in (c). The incident and reflected acoustic pulses in the time domain are shown in (d).

supporting the piezoelectric layers from the edge. The unmatched transducer was fabricated by first soldering a coaxial cable to the back of the piezoelectric transducer (Steminc SMD30T21F1000R). The transducer was mounted in the casing, as shown in Fig. 4a, and the gaps were sealed using 3M DP100 epoxy.

The matched transducers (Fig. 4b) were fabricated by first bonding a 1 1/4" x 1/16" fused quartz glass disc, supplied by TGP Inc. ($\rho_1 = 2200 \text{ kg m}^{-3}$, $c_1 = 5500 \text{ m s}^{-1}$, $Z_1 = 12.1 \text{ MRayl}$, $\alpha_1 = 5 \text{ dB/m/MHz}$) [59], to the front face of the piezoelectric transducer through a vacuum bonding process. The thickness of the glass disk 1/16" (1.56 mm) is

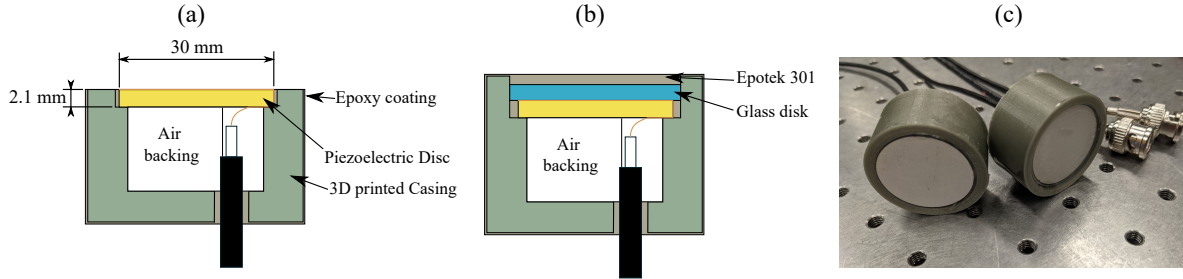


Figure 4. (a) Schematic of an air-backed transducer without acoustic matching layers. (b) Construction of the two-layer acoustically matched transducer. (c) Fabricated transducers U1 and M1 before polishing.

slightly larger than the quarter wavelength thickness at 1 MHz (1.43 mm). A coaxial cable was soldered to the piezoelectric disc, and the transducer/glass assembly was mounted inside the casing. The casing was designed so that the remaining height acts as a mold for the epoxy matching layer. The transducer was sealed and coated using Epotek 301 epoxy ($\rho_2 = 1090 \text{ kg m}^{-3}$, $c_2 = 2640 \text{ m s}^{-1}$, $Z_2 = 2.85 \text{ MRayl}$, $\alpha_2 = 250 \text{ dB/m/MHz}$) [59], and a heat gun was used to ensure that no air bubbles remained trapped in the epoxy layer before leaving it to cure for 24 hours. The cured layer was then sanded down till it was flush with the front of the casing using 200 grit sandpaper followed by 400 grit, then 600 grit. The fabricated transducers are shown in Fig. 4c.

4.2. Measuring the Electrical Impedance of the Transducers

An Agilent 33250A signal generator and a Tektronix TDS5034B oscilloscope were used to measure the electrical impedance of the fabricated transducers experimentally. The signal generator was connected to the tested transducer and then programmed to apply a voltage chirp signal that swept from 100 kHz up to 2 MHz. The applied voltage and the current flowing to the transducer were measured simultaneously using a 10x 150 MHz voltage probe and a current probe (Tektronix P6022). The voltage and current signals were then converted to the frequency domain and used to calculate the input electrical impedance of the transducer.

The electrical impedance of an unmatched transducer in air was first used to estimate the exact piezoelectric material properties using the procedure described in Ref. [60]. The experimentally measured piezoelectric properties are summarized in Table 3.

The transducers' electrical impedance was measured underwater in a 30"x20"x15" water tank. The experimental electric impedance of the different transducers is compared to the analytical predictions in Fig. 5. The experimental results agree well with the analytical predictions with a slight deviation caused by the uncertainties in the material properties and geometry of the different layers. The acoustic matching of the transducer was sensitive to the thickness of the glass and epoxy layers, as shown

Table 3. Experimentally identified modified PZT-4 material properties from electrical impedance data in air.

Property	ρ_p	c_p	\bar{h}_{33}	C_{33}^D	C_p	Q_m	$\tan \delta$
Unit	kg/m ³	m/s	kV/mm	GPa	nF	-	%
Value	7900	4714	2313	175	2.4	500	0.4

by circle size difference between transducers M1 to M3. A better acoustic impedance match can be achieved by fine-tuning the glass and epoxy layers geometry as predicted in Fig. 3. Transducer M3 showed the best acoustic matching (smallest circle in the Smith chart), so it was selected for subsequent electrical impedance matching.

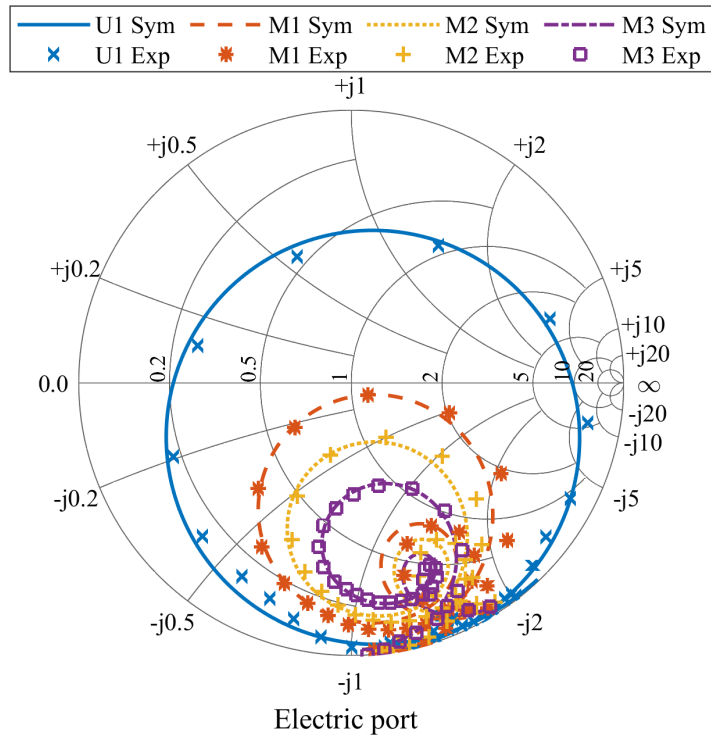


Figure 5. Analytical (lines) and experimental (markers) electric impedance for three matched transducers (M1-M3) with different epoxy layer thickness as summarized in Table 2. The impedance of a transducer without acoustic matching (U1) is shown for reference.

4.3. Setup for Measuring the Acoustic Reflection Coefficient

The acoustic reflection coefficient of the fabricated transducers was measured using the setup shown in Fig. 6. A Panametrics 5800 pulser/receiver was used to excite a

broadband Olympus V394 source transducer. The reflected echo signal at the source transducer was filtered and amplified by the pulser and routed to an oscilloscope for display and recording. The pulser was set to excite the transducer with a $12.5 \mu\text{J}$ pulse with a repetition rate of 500 Hz. The echo signal was filtered with a 100 kHz-10 MHz bandpass filter to reduce the noise then amplified with a 20 dB gain.

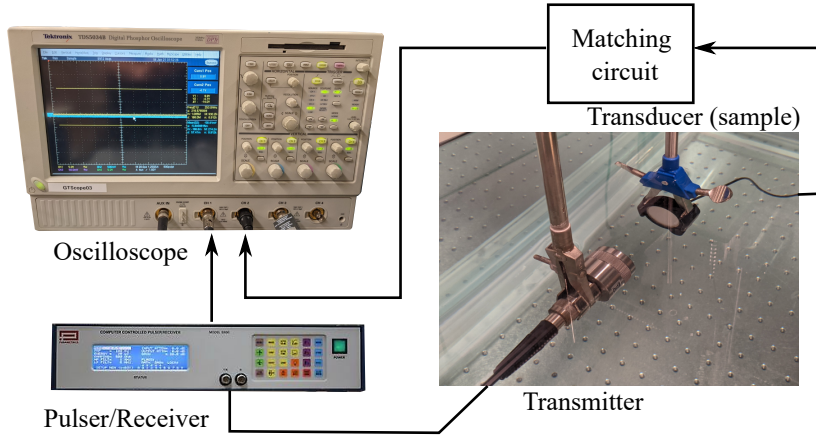


Figure 6. Experimental setup for measuring the acoustic reflection coefficient of the fabricated transducers.

The acoustic reflection coefficient of the samples was calibrated using the echo from normal incidence on a stainless-steel 304 cylinder of 26.4 mm thickness and 101 mm diameter. Normal incidence was verified by rotating the calibration cylinder until the maximum echo amplitude was achieved. The first echo from the calibration cylinder was windowed and then converted to the frequency domain. The acoustic reflection coefficient from the sample was then calculated using the relation:

$$S_{11} = R_{st} \frac{A_{sample}}{A_{calib}} \quad (11)$$

where A_{sample} is the reflected signal from the sample, A_{calib} is the reflected signal from the stainless-steel cylinder, and R_{st} is the reflection coefficient of a water-steel interface calculated from:

$$R_{st} = \frac{Z_{st} - Z_w}{Z_{st} + Z_w} \quad (12)$$

where $Z_{st} = 46.57 \text{ MRayl}$ is the acoustic impedance of stainless steel.

The experimental acoustic reflection coefficients for the unmatched and matched transducers (U1 and M3) are compared to the analytical models in Fig. 7. The reflection coefficient is measured and simulated with respect to a 50Ω output for both samples, i.e., no electrical matching was done for this measurement. For both samples, the amplitude of the experimental reflection coefficient is lower than the simulations for all frequencies. This shift is caused by unmodeled losses due to diffraction and misalignment between the transducers.

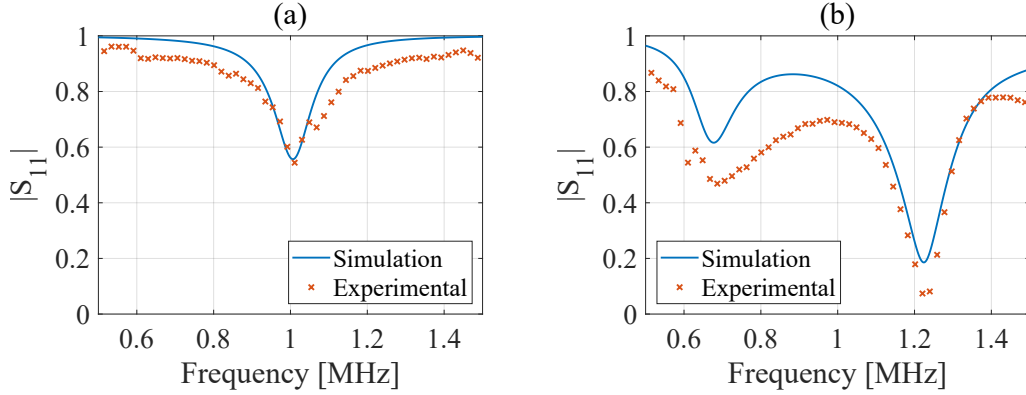


Figure 7. Experimental versus analytical acoustic reflection coefficient for (a) the transducer without acoustic matching (U1), and (b) the two-layer acoustically matched transducer (M3).

The two-layer acoustically matched transducer M3 was first electrically matched to achieve maximum bandwidth while connected to a 50Ω electric load. The four-element electrical matching network shown in Fig. 8 was designed and optimized using the impedance matching tool in Keysight Advanced Design System (ADS) software. The random optimization algorithm built into the software was used to minimize S_{22} for the frequency bandwidth between 0.5 MHz and 1.5 MHz. The four-element circuit was used instead of the two-element circuit proposed in Sec. 3 due to the imperfections in the acoustic matching caused by the geometrical and material uncertainty.

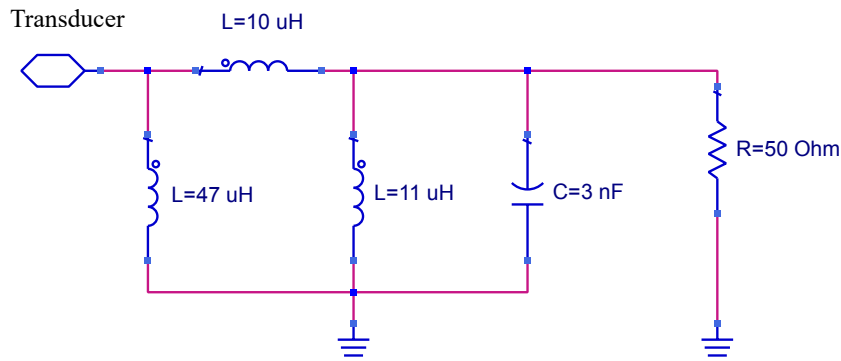


Figure 8. Electrical circuit used to achieve broadband electrical impedance matching for the acoustically matched transducer (M3).

The experimental acoustic reflection from the transducer with the matching circuit is compared to open circuit termination in Fig. 9. The matched transducer achieved up to 70% bandwidth centered around 900 kHz with a factor of 3 change in amplitude (10 dB) between the open circuit and matched states, as shown in Fig. 9a. Considering the modulation of the echo signal shown in Fig. 9b, at least 200 kbps of data can be transmitted using this setup with simple amplitude shift keying (ASK) modulation. Higher data rates are possible with advanced modulation techniques such as OFDM.

It should be noted that the echo signal in Fig. 9b is different than that estimated analytically in Fig. 3d for two reasons. First, the signal plotted in Fig. 9b is for the voltage signal captured by the transmitter not the actual reflected pressure signal, i.e., the signal is multiplied by the two-way transfer function of the transmitter. Second, the impedance matching in Fig. 3 is different from that implemented experimentally due to the uncertainties in the acoustic matching.

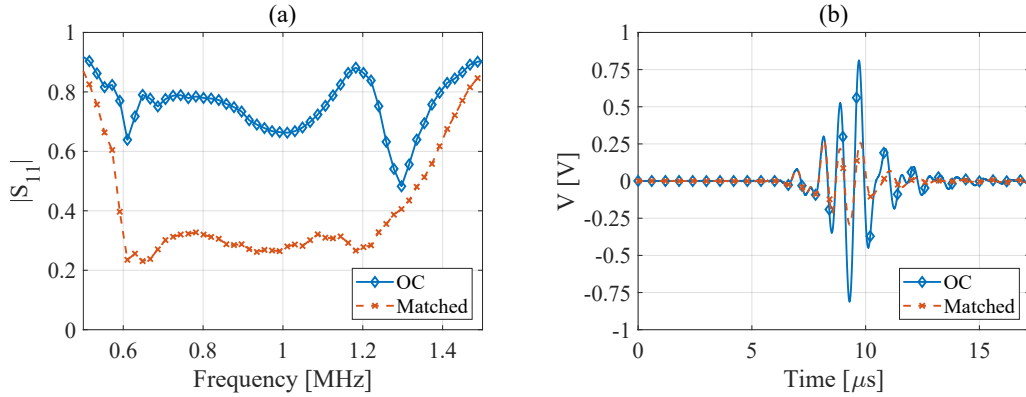


Figure 9. (a) Experimental acoustic reflection coefficient for an electrically and acoustically matched transducer. Broadband electrical matching is shown using the circuit in Fig. 8 versus when the transducer was open circuit. (b) Time waveform showing the modulation of the reflected pulse by varying electrical circuit connected to the transducer.

5. Impedance Matching for Simultaneous Power and Data Transfer

The matched transducer can be designed to receive power while transmitting data simultaneously by dividing its wide bandwidth between a narrowband power channel and a broadband data channel. This frequency multiplexing is realized using the circuit shown in Fig. 10. It is a frequency splitter designed to direct incident data signals with frequencies between 600 kHz and 900 kHz to a dummy communication load while directing the power signal (sent continuously at 1.3 MHz) to a power harvesting circuit. The splitter is realized using a series LC circuit as a narrow bandpass filter for the power signal. A second parallel LC circuit is used as a bandstop filter to pass all frequencies to a communication load except for the power frequency (1.3 MHz). The bandwidth of the bandstop further is improved by adding a parallel capacitor for matching to the 50Ω load. By switching the data branch on and off, incident signal at data frequencies is modulated while the power signal is continuously fed to an energy harvesting circuit for powering the wireless device.

The circuit in Fig. 10b was implemented on a breadboard, and the experimental acoustic reflection coefficient was measured as shown in Fig. 11a. The communication branch is switched to transmit backscatter communication signal in the frequency range

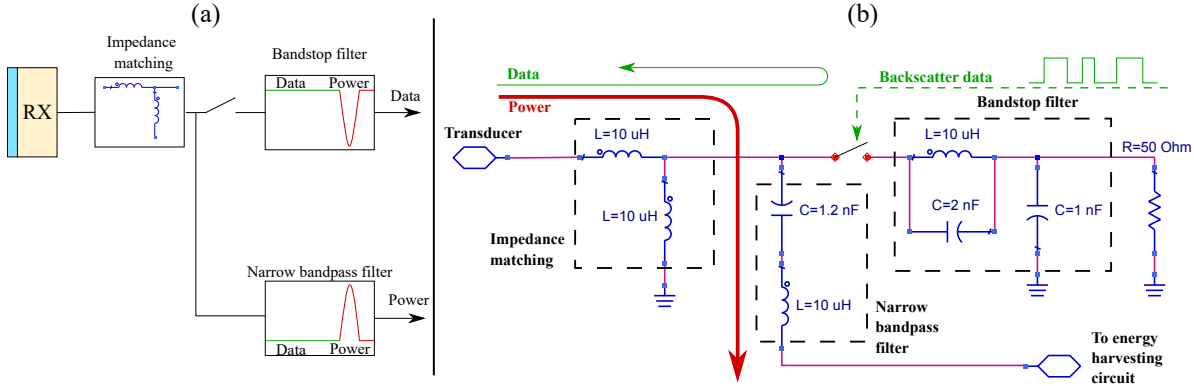


Figure 10. (a) Schematic and (b) implementation of an electrical circuit for simultaneous ultrasonic power and data transfer. The circuit routes incident power and data signals to two separate electrical branches allowing for uninterrupted power flow to an energy harvesting circuit while transmitting backscatter data.

between 600 kHz and 900 kHz. The power branch at 1.3 MHz is not affected by the communication signal and almost all the power incident on the transducer at this frequency is absorbed.

The normalized spectrum of the voltage signals received at the different branches of the system are shown in Fig. 11b. The communication branch load absorbs the incident power in the data channel frequency range (600 kHz-900 kHz) while rejecting the power signal above 1 MHz. The time signal for the echo received by the transmitter filtered in the data channel bandwidth between 600 kHz and 900 kHz is shown in Fig. 11c. The difference between the amplitude of the two communication states is more than the double (6 dB), demonstrating high sensitivity.

The circuit shown in Fig. 11b was constructed using the fewest number of nominal inductor and capacitor values. The upper bound of the data bandwidth is limited by a guard band between the power and data channels that prevents power from leaking to the data band. The data bandwidth can be enhanced further using a higher order matching filter with more number of elements which allows for a narrower buffer zone. The power branch absorbs power most efficiently around the target frequency of 1.3 MHz, as indicated by the low reflection coefficient in Fig. 11a. The sensitivity of the power branch is higher than the data branch due to its narrowband nature.

Several modifications to the electrical matching circuit is possible depending on the target application. For example, (1) the reliability of the power transfer can be improved by increasing its bandwidth while sacrificing some sensitivity and efficiency using a higher order filtering topology. (2) The data and power frequency channels can be swapped to allow for power transfer at lower frequencies (around 700 kHz) by modifying the filters' target frequencies. The power transmission frequency can be chosen to maximize the efficiency depending on the distance between the transmitter and the receiver, i.e., whether the system is limited by divergence losses (wave spreading) or attenuation. The matching filters used can be tweaked for allocating the power and data

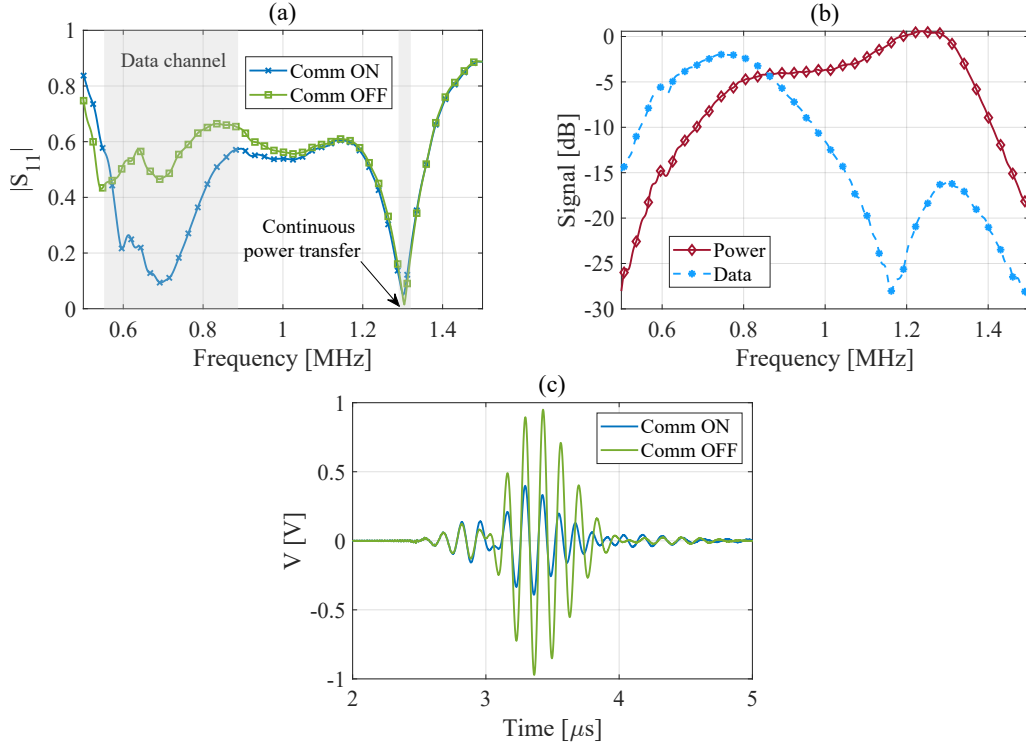


Figure 11. (a) Experimental acoustic reflection coefficient for a transducer connected to the simultaneous power and data transfer circuit shown in Fig. 8. (b) The spectrum of the signal received by the power branch of the circuit versus that received by the data branch for an incident ultrasonic pulse. (c) Filtered echo signal showing the data bandwidth between 600 kHz and 800 kHz.

bands within the transducer bandwidth limited by the quality of the acoustic impedance matching. (3) The current implementation focused on the fundamental frequency of the piezoelectric transducer as a proof of concept; however, a larger bandwidth is available if the frequencies surrounding the odd harmonics of the piezoelectric transducer are considered. Finally, (4) the power received at the data channel when it is absorbing incident power (transmitting a zero by not reflecting the incident acoustic power) may also be routed to the energy harvesting circuit to increase the power harvested by the system.

6. Conclusions

A piezoelectric transducer was designed for maximum operating bandwidth while maintaining a high sensitivity. The transducer was matched acoustically using two quarter-wavelength layers and electrically using a 4-element wideband matching circuit. Experimental characterization of the transducer verified a 600 kHz (70%) bandwidth with a 10 dB difference between connecting the matching circuit and keeping the transducer open, allowing for reliable backscatter communication with high data rates.

A technique for simultaneous underwater power and data transfer using a single transducer was developed and experimentally validated. The power and data signals were multiplexed to ensure uninterrupted power transmission to an underwater wireless sensor maintaining backscatter communication with large data bandwidth. A high sensitivity data bandwidth of 300 kHz was obtained while achieving uninterrupted power transfer with minimum reflection. A simultaneous ultrasonic power and data transfer system prototype is currently being developed to characterize the efficiency, delivered power, range, data throughput, and error rate using this technique. The developed technique has applications in biomedical implants, ocean monitoring and navigation, and through-metal ultrasonic transfer for shielded devices and enclosures.

Acknowledgment

The authors acknowledge support from U.S. National Science Foundation CMMI Grant No. 1727951.

References

- [1] Dongjin Seo, Ryan M. Neely, Konlin Shen, Utkarsh Singhal, Elad Alon, Jan M. Rabaey, Jose M. Carmena, and Michel M. Maharbiz. Wireless Recording in the Peripheral Nervous System with Ultrasonic Neural Dust. *Neuron*, 91(3):529–539, August 2016.
- [2] Tristan J. Lawry, Kyle R. Wilt, Jon D. Ashdown, Henry A. Scarton, and Gary J. Saulnier. A high-performance ultrasonic system for the simultaneous transmission of data and power through solid metal barriers. *IEEE Transactions on Ultrasonics, Ferroelectrics, and Frequency Control*, 60(1):194–203, January 2013.
- [3] Junsu Jang and Fadel Adib. Underwater backscatter networking. In *SIGCOMM ’19: Proceedings of the ACM Special Interest Group on Data Communication*, pages 187–199, Beijing, China, August 2019. ACM.
- [4] R. Guida, E. Demirors, N. Dave, and T. Melodia. Underwater Ultrasonic Wireless Power Transfer: A Battery-less Platform for the Internet of Underwater Things. *IEEE Transactions on Mobile Computing*, pages 1–1, 2020.
- [5] Hamid Basaeri, David B Christensen, and Shad Roundy. A review of acoustic power transfer for bio-medical implants. *Smart Materials and Structures*, 25(12):123001, December 2016.
- [6] Francesco Mazzilli, Michela Peisino, Rostand Mitouassiwou, Benjamin Cotté, Prakash Thoppay, Cyril Lafon, Patrick Favre, Eric Meurville, and Catherine Dehollain. In-vitro platform to study ultrasound as source for wireless energy transfer and communication for implanted medical devices. In *2010 Annual International Conference of the IEEE Engineering in Medicine and Biology*, pages 3751–3754, August 2010.
- [7] Francesco Mazzilli, Cyril Lafon, and Catherine Dehollain. A 10.5 cm Ultrasound Link for Deep Implanted Medical Devices. *IEEE Transactions on Biomedical Circuits and Systems*, 8(5):738–750, October 2014.
- [8] Marcus J. Weber, Yoshiaki Yoshihara, Ahmed Sawaby, Jayant Charthad, Ting Chia Chang, and Amin Arbabian. A Miniaturized Single-Transducer Implantable Pressure Sensor With Time- Multiplexed Ultrasonic Data and Power Links. *IEEE Journal of Solid-State Circuits*, 53(4):1089–1101, April 2018.
- [9] Monzurul Alam, Shuai Li, Rakib Uddin Ahmed, Yat Man Yam, Suman Thakur, Xiao-Yun Wang, Dan Tang, Serena Ng, and Yong-Ping Zheng. Development of a battery-free ultrasonically

- powered functional electrical stimulator for movement restoration after paralyzing spinal cord injury. *Journal of NeuroEngineering and Rehabilitation*, 16(1):36, March 2019.
- [10] Chen Shi, Victoria Andino-Pavlovsky, Stephen A. Lee, Tiago Costa, Jeffrey Elloian, Elisa E. Konofagou, and Kenneth L. Shepard. Application of a sub-0.1-mm³ implantable mote for in vivo real-time wireless temperature sensing. *Science Advances*, 7(19):eabf6312, May 2021.
 - [11] B. Gil, S. Anastasova, and G. Z. Yang. Low-powered implantable devices activated by ultrasonic energy transfer for physiological monitoring in soft tissue via functionalized electrochemical electrodes. *Biosensors and Bioelectronics*, 182:113175, June 2021.
 - [12] Teimour Maleki, Ning Cao, Seung Hyun Song, Chinghai Kao, Song-Chu Ko, and Babak Ziaie. An Ultrasonically Powered Implantable Micro-Oxygen Generator (IMOGEN). *IEEE Transactions on Biomedical Engineering*, 58(11):3104–3111, November 2011.
 - [13] Albert Kim, Jiawei Zhou, Shayak Samaddar, Seung Hyun Song, Bennet D. Elzey, David H. Thompson, and Babak Ziaie. An Implantable Ultrasonically-Powered Micro-Light-Source (μ Light) for Photodynamic Therapy. *Sci Rep*, 9(1):1395, February 2019.
 - [14] D. K. Piech, J. E. Kay, B. E. Boser, and M. M. Maharbiz. Rodent wearable ultrasound system for wireless neural recording. In *2017 39th Annual International Conference of the IEEE Engineering in Medicine and Biology Society (EMBC)*, pages 221–225, July 2017.
 - [15] J.-Y. Tsai, K.-H. Huang, J.-R. Wang, S.-I. Liu, and P.-C. Li. Ultrasonic wireless power and data communication for neural stimulation. In *2011 IEEE International Ultrasonics Symposium*, pages 1052–1055, October 2011.
 - [16] Ye-Sing Luo, Jiun-Ru Wang, Wei-Jen Huang, Je-Yu Tsai, Yi-Fang Liao, Wan-Ting Tseng, Chen-Tung Yen, Pai-Chi Li, and Shen-Iuan Liu. Ultrasonic Power/Data Telemetry and Neural Stimulator With OOK-PM Signaling. *IEEE Transactions on Circuits and Systems II: Express Briefs*, 60(12):827–831, December 2013.
 - [17] Jayant Charthad, Marcus J. Weber, Ting Chia Chang, and Amin Arbabian. A mm-Sized Implantable Medical Device (IMD) With Ultrasonic Power Transfer and a Hybrid Bi-Directional Data Link. *IEEE Journal of Solid-State Circuits*, 50(8):1741–1753, August 2015.
 - [18] Jayant Charthad, Ting Chia Chang, Zhaokai Liu, Ahmed Sawaby, Marcus J. Weber, Sam Baker, Felicity Gore, Stephen A. Felt, and Amin Arbabian. A mm-Sized Wireless Implantable Device for Electrical Stimulation of Peripheral Nerves. *IEEE Transactions on Biomedical Circuits and Systems*, 12(2):257–270, April 2018.
 - [19] Byunghun Lee, Mukhesh K. Koripalli, Yaoyao Jia, Joshua Acosta, M. S. E. Sendi, Yoonsu Choi, and Maysam Ghovanloo. An Implantable Peripheral Nerve Recording and Stimulation System for Experiments on Freely Moving Animal Subjects. *Sci Rep*, 8(1):6115, April 2018.
 - [20] Lucia Tacchetti, Wouter A. Serdijn, and Vasiliki Giagka. An Ultrasonically Powered and Controlled Ultra-High-Frequency Biphasic Electrical Neurostimulator. In *2018 IEEE Biomedical Circuits and Systems Conference (BioCAS)*, pages 1–4, October 2018.
 - [21] David K. Piech, Benjamin C. Johnson, Konlin Shen, M. Meraj Ghanbari, Ka Yiu Li, Ryan M. Neely, Joshua E. Kay, Jose M. Carmena, Michel M. Maharbiz, and Rikky Muller. A wireless millimetre-scale implantable neural stimulator with ultrasonically powered bidirectional communication. *Nat Biomed Eng*, 4(2):207–222, February 2020.
 - [22] FDA. Marketing Clearance of Diagnostic Ultrasound Systems and Transducers. Technical Report FDA-2017-D-5372, Federal Drug & Food Administration, June 2019.
 - [23] MirHojjat Seyed, Behailu Kibret, Daniel T. H. Lai, and Michael Faulkner. A Survey on Intrabody Communications for Body Area Network Applications. *IEEE Transactions on Biomedical Engineering*, 60(8):2067–2079, August 2013.
 - [24] Banafsaj Jaafar, Junwen Luo, Dimitrios Firfillionis, Ahmed Soltan, Jeff Neasham, and Patrick Degenaar. Ultrasound Intra Body Multi Node Communication System for Bioelectronic Medicine. *Sensors*, 20(1):31, January 2020.

- [25] John Heidemann, Milica Stojanovic, and Michele Zorzi. Underwater sensor networks: Applications, advances and challenges. *Philosophical Transactions of the Royal Society A: Mathematical, Physical and Engineering Sciences*, 370(1958):158–175, January 2012.
- [26] Liu Lanbo, Zhou Shengli, and Cui Jun-Hong. Prospects and problems of wireless communication for underwater sensor networks. *Wireless Communications and Mobile Computing*, 8(8):977–994, 2008.
- [27] Jaime Lloret. Underwater Sensor Nodes and Networks. *Sensors*, 13(9):11782–11796, September 2013.
- [28] Jay Pearlman, Simon Jirka, Joaquin del Rio, Eric Delory, Lennard Frommhold, Sergio Martinez, and Tom O'Reilly. Oceans of Tomorrow sensor interoperability for in-situ ocean monitoring. In *OCEANS 2016 MTS/IEEE Monterey*, pages 1–8, September 2016.
- [29] Milica Stojanovic. On the relationship between capacity and distance in an underwater acoustic communication channel. *SIGMOBILE Mob. Comput. Commun. Rev.*, 11(4):34–43, October 2007.
- [30] Christopher G Lowe, Kim N Holland, and Thomas G Wolcott. A new acoustic tailbeat transmitter for fishes. *Fisheries Research*, 36(2):275–283, June 1998.
- [31] Martin Føre, Jo Arve Alfredsen, and Aage Grønningssater. Development of two telemetry-based systems for monitoring the feeding behaviour of Atlantic salmon (*Salmo salar* L.) in aquaculture sea-cages. *Computers and Electronics in Agriculture*, 76(2):240–251, May 2011.
- [32] Huidong Li, Chuan Tian, Jun Lu, Mitchell J. Myjak, Jayson J. Martinez, Richard S. Brown, and Zhiqun Daniel Deng. An Energy Harvesting Underwater Acoustic Transmitter for Aquatic Animals. *Sci Rep*, 6(1):33804, September 2016.
- [33] Liam Paull, Sajad Saeedi, Mae Seto, and Howard Li. AUV Navigation and Localization: A Review. *IEEE Journal of Oceanic Engineering*, 39(1):131–149, January 2014.
- [34] Reza Ghaffarivardavagh, Sayed Saad Afzal, Osvaldo Rodriguez, and Fadel Adib. Ultra-Wideband Underwater Backscatter via Piezoelectric Metamaterials. In *Proceedings of the Annual Conference of the ACM Special Interest Group on Data Communication on the Applications, Technologies, Architectures, and Protocols for Computer Communication*, SIGCOMM '20, pages 722–734, New York, NY, USA, July 2020. Association for Computing Machinery.
- [35] R. Guida, E. Demirors, N. Dave, J. Rodowicz, and T. Melodia. An Acoustically Powered Battery-less Internet of Underwater Things Platform. In *2018 Fourth Underwater Communications and Networking Conference (UComms)*, pages 1–5, August 2018.
- [36] D. A. Shoudy, G. J. Saulnier, H. A. Scarton, P. K. Das, S. Roa-Prada, J. D. Ashdown, and A. J. Gavens. An Ultrasonic Through-Wall Communication System with Power Harvesting. In *2007 IEEE Ultrasonics Symposium Proceedings*, pages 1848–1853, October 2007.
- [37] M. Kluge, Th. Becker, J. Schalk, and T. Otterpohl. Remote acoustic powering and data transmission for sensors inside of conductive envelopes. In *2008 IEEE SENSORS*, pages 41–44, October 2008.
- [38] David J. Graham, Jeffrey A. Neasham, and Bayan S. Sharif. Investigation of Methods for Data Communication and Power Delivery Through Metals. *IEEE Transactions on Industrial Electronics*, 58(10):4972–4980, October 2011.
- [39] T. J. Lawry, G. J. Saulnier, J. D. Ashdown, K. R. Wilt, H. A. Scarton, S. Pascarelle, and J. D. Pinezich. Penetration-free system for transmission of data and power through solid metal barriers. In *2011 - MILCOM 2011 Military Communications Conference*, pages 389–395, November 2011.
- [40] Jonathan D. Ashdown, Kyle R. Wilt, Tristan J. Lawry, Gary J. Saulnier, David A. Shoudy, Henry A. Scarton, and Andrew J. Gavens. A full-duplex ultrasonic through-wall communication and power delivery system. *IEEE Transactions on Ultrasonics, Ferroelectrics, and Frequency Control*, 60(3):587–595, March 2013.

- [41] Victor Farm-Guoo Tseng, Sarah S. Bedair, and Nathan Lazarus. Acoustic Power Transfer and Communication With a Wireless Sensor Embedded Within Metal. *IEEE Sensors Journal*, 18(13):5550–5558, July 2018.
- [42] Victor L. Takahashi, Alan C. Kubrusly, Arthur M. B. Braga, Sully M. M. Quintero, Sávio W. O. Figueiredo, and Ana B. Domingues. Ultrasonic Power and Data Transfer through Multiple Curved Layers Applied to Pipe Instrumentation. *Sensors*, 19(19):4074, January 2019.
- [43] X. Tang, M. Sameer, and S. Mandal. Acoustic Wireless Power and Data Telemetry for Structural Health Monitoring. In *2018 IEEE SENSORS*, pages 1–4, October 2018.
- [44] Sebastian Roa-Prada, Henry A. Scarton, Gary J. Saulnier, David A. Shoudy, Jonathan D. Ashdown, Pankaj K. Das, and Andrew J. Gavens. An Ultrasonic Through-Wall Communication (UTWC) System Model. *Journal of Vibration and Acoustics*, 135(011004), February 2013.
- [45] Shaul Ozeri and Doron Shmilovitz. Simultaneous backward data transmission and power harvesting in an ultrasonic transcutaneous energy transfer link employing acoustically dependent electric impedance modulation. *Ultrasonics*, 54(7):1929–1937, September 2014.
- [46] Bruno M. G. Rosa and Guang Z. Yang. Towards Integration of Ultrasonic-Powered Implantable Devices for Physiological Monitoring, Stimulation, and Imaging in Soft Tissues Using a Handheld Scanning Probe. *IEEE Sensors Journal*, pages 1–1, 2020.
- [47] Shin-nosuke Suzuki, Shunsuke Kimura, Tamotsu Katane, Hideo Saotome, Osami Saito, and Kazuhito Kobayashi. Power and Interactive Information Transmission to Implanted Medical Device Using Ultrasonic. *Jpn. J. Appl. Phys.*, 41(5S):3600, May 2002.
- [48] Hideyuki Kawanabe, Tamotsu Katane, Hideo Saotome, Osami Saito, and Kazuhito Kobayashi. Power and Information Transmission to Implanted Medical Device Using Ultrasonic. *Jpn. J. Appl. Phys.*, 40(5S):3865, May 2001.
- [49] G. J. Saulnier, H. A. Scarton, A. J. Gavens, D. A. Shoudy, T. L. Murphy, M. Wetzel, S. Bard, S. Roa-Prada, and P. Das. P1G-4 Through-Wall Communication of Low-Rate Digital Data Using Ultrasound. In *2006 IEEE Ultrasonics Symposium*, pages 1385–1389, October 2006.
- [50] Martin Kluge, Jordi Sabater, Josef Schalk, Luong V. Ngo, Helmut Seidel, and Ulrich Schmid. Wireless Sensing of Physical Parameters Inside Hermetically Enclosed Conductive Envelopes. In *ASME 2007 International Design Engineering Technical Conferences and Computers and Information in Engineering Conference*, pages 353–359. American Society of Mechanical Engineers Digital Collection, September 2007.
- [51] Benjamin C. Johnson, Konlin Shen, David Piech, M. Meraj Ghanbari, Ka Yiu Li, Ryan Neely, Jose M. Carmena, Michel M. Maharbiz, and Rikky Muller. StimDust: A 6.5mm³, wireless ultrasonic peripheral nerve stimulator with 82% peak chip efficiency. In *2018 IEEE Custom Integrated Circuits Conference (CICC)*, pages 1–4, April 2018.
- [52] Gordon S. Kino. *Acoustic Waves: Devices, Imaging, and Analog Signal Processing*. Prentice Hall, Englewood Cliffs, N.J, January 1987.
- [53] Tristan J. Lawry, Kyle R. Wilt, Henry A. Scarton, and Gary J. Saulnier. Analytical modeling of a sandwiched plate piezoelectric transformer-based acoustic-electric transmission channel. *IEEE Transactions on Ultrasonics, Ferroelectrics, and Frequency Control*, 59(11):2476–2486, November 2012.
- [54] Clive Poole and Izzat Darwazeh. *Microwave Active Circuit Analysis and Design*. Academic Press, Oxford, January 2016.
- [55] Vivek T. Rathod. A Review of Acoustic Impedance Matching Techniques for Piezoelectric Sensors and Transducers. *Sensors*, 20(14):4051, January 2020.
- [56] Marjan Bakhtiari-Nejad, Muhammad R. Hajj, and Shima Shahab. Dynamics of acoustic impedance matching layers in contactless ultrasonic power transfer systems. *Smart Mater. Struct.*, 29(3):035037, February 2020.
- [57] J.H. Goll and B.A. Auld. Multilayer Impedance Matching Schemes for Broadbanding of Water Loaded Piezoelectric Transducers and High Q Electric Resonators. *IEEE Transactions on Sonics and Ultrasonics*, 22(1):52–53, January 1975.

- [58] T. E. G. Alvarez-Arenas. Acoustic impedance matching of piezoelectric transducers to the air. *IEEE Transactions on Ultrasonics, Ferroelectrics, and Frequency Control*, 51(5):624–633, May 2004.
- [59] A.R. Selfridge. Approximate Material Properties in Isotropic Materials. *IEEE Transactions on Sonics and Ultrasonics*, 32(3):381–394, May 1985.
- [60] Charles H. Sherman and John L. Butler. *Transducers and Arrays for Underwater Sound*. Springer New York, New York, NY, 2007.